

## Controlling Network Structure in Degradable Thiol–Acrylate Biomaterials to Tune Mass Loss Behavior

Amber E. Rydholm,<sup>†</sup> Sirish K. Reddy,<sup>†</sup> Kristi S. Anseth,<sup>†,‡</sup> and Christopher N. Bowman<sup>\*,†,§</sup>

Department of Chemical and Biological Engineering, University of Colorado, Boulder, Colorado 80309-0424, Howard Hughes Medical Institute, University of Colorado, Boulder, Colorado 80309-0424, and Department of Restorative Dentistry, University of Colorado Health Sciences Center, Denver, Colorado 80045-0508

Received April 18, 2006; Revised Manuscript Received August 2, 2006

Degradable thiol–acrylate materials were synthesized from the mixed-mode polymerization of a diacrylate poly(ethylene glycol) (PEG) monomer with thiol monomers of varying functionalities to control the final network structure, ultimately influencing the material's degradation behavior and properties. The influence of the concentration of thiol groups and monomer functionality on the mass loss profiles were examined experimentally and theoretically. Mass loss behavior was also predicted for networks with varying extents of cyclization, PEG molecular weight, and backbone chain length distributions. Experimental results indicate that increasing the thiol concentration from 10 to 50 mol % shifted the reverse gelation time from 35 to 8 days and the extent of mass loss at reverse gelation from 75 to 40%. Similarly, decreasing the thiol functionality from 4 to 1 shifted the reverse gelation time from 18 to 8 days and the mass loss extent at reverse gelation from 70 to 45%.

### Introduction

Degradable networks formed from the photopolymerization of multifunctional monomers are an emerging class of biomaterials with unique advantages related to the ability to process these materials under physiological conditions in the presence of tissues, cells, and even DNA.<sup>1–7</sup> These biomaterial networks are being investigated for numerous applications, especially in the fields of drug delivery and tissue engineering.<sup>4,7–20</sup> However, major limitations exist with respect to controlling the network degradation and mass loss profiles, which further impact the structure-dependent material properties. The ability to tailor a single polymer system to meet the requirements of an array of biomaterial applications would be a major advantage.

Degradation in covalently cross-linked polymer networks is influenced by the network chemistry, the cross-link chemistry, and by network structure. The bulk network chemistry influences network swelling and internal water concentrations, the local cross-link chemistry impacts the rate of cross-link cleavage during degradation, and network structure influences how the degradation of individual cross-links impacts the overall mass loss behavior. Using chemistry to control degradation requires the design and synthesis of new monomers, which is often a lengthy process. Alternatively, controlling network structure at the molecular level can be as simple as manipulating monomer molecular weight, functionality, or concentration.<sup>21–23</sup> Understanding how the polymer network structure changes temporally throughout degradation would significantly improve our ability

to control the diffusivity, permeability, equilibrium water content, elasticity, and modulus<sup>24</sup> of the bulk material.

Monomer molecular weight, functionality, concentration, and the polymerization mechanism all contribute to polymer network structure. Three photoinitiated radical polymerization mechanisms are used to form covalently cross-linked polymers: chain growth, step growth, and mixed chain and step growth. While numerous examples of in situ forming polymeric biomaterials created from both chain growth- and step growth-type mechanisms exist,<sup>13,21,25–29</sup> relatively few publications have explored degradable polymers resulting from a mixed-mode polymerization mechanism.<sup>30–32</sup>

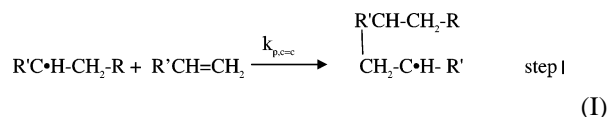
Here, we will focus on polymer networks produced from the photopolymerization of a unique combination of a multifunctional thiol monomer and a multifunctional acrylate monomer. This combination leads to a mixed step and chain growth polymerization reaction.<sup>33</sup> During thiol–acrylate polymerization, the acrylic radical participates in two reactions: addition to another acrylate functional group (step I) or hydrogen abstraction/chain transfer to thiol (step III). In contrast, thiyl radicals generated by hydrogen abstraction are only able to propagate through another acrylate carbon–carbon double bond (step II) to regenerate an acrylic radical. The network structure in degradable thiol–acrylate materials is comprised of thiol–polyacrylate backbone chains that are connected to each other through degradable cross-links. The distribution of the thiol–polyacrylate backbone chain lengths is controlled through the thiol functionality, the ratio of thiol and acrylate functional groups in the initial monomer mixture, and the amount of acrylate homopolymerization that occurs (step I) relative to chain transfer to thiol (step III).<sup>31</sup>

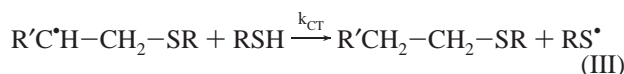
\* To whom correspondence should be addressed. Address: Engineering Center, Room ECCH 111, Department of Chemical and Biological Engineering, Campus Box 424, University of Colorado, Boulder, CO 80309-0424, USA. Tel: +1-303-492-3247; fax: +1-303-492-4341. E-mail address: bowmanc@colorado.edu.

<sup>†</sup> Department of Chemical and Biological Engineering, University of Colorado.

<sup>‡</sup> Howard Hughes Medical Institute, University of Colorado.

<sup>§</sup> University of Colorado Health Sciences Center.





Previous researchers<sup>33</sup> developed a comprehensive model based on these reactions that captures the polymerization kinetics. The ratio of propagation to chain transfer kinetic constants ( $k_{p,c=c}/k_{CT}$ ) was found to be approximately 1.5 for several nondegradable thiol–acrylate systems. Expanding upon this understanding of thiol–acrylate polymerization, Reddy et al. predicted the distribution of thiol–polyacrylate backbone chains and mass loss behavior for a variety of networks.<sup>31</sup> Included in this detailed analysis of theoretical systems was an evaluation of the influence of thiol functionality and concentration on mass loss profiles for the resulting polymers.

In the work presented herein, experimental thiol–acrylate mass loss profiles are compared to the results of Reddy's theoretical model. Cross-linked networks were photopolymerized from mixtures of a poly(ethylene glycol) (PEG)–poly(lactic acid) (PLA) diacrylate and commercially available mono-, di-, and tetrathiol monomers. Accurate prediction of the mass loss profiles for these networks requires an understanding of both the rate of ester hydrolysis in the degradable PEG–PLA cross-links ( $k_{hyd}$ ) and the distribution of the thiol–polyacrylate backbone chains. The first parameter was determined experimentally from equilibrium mass swelling ratios measured throughout the network degradation. The thiol–polyacrylate chain length distribution was predicted using  $k_{p,c=c}/k_{CT}$  ratios determined from the polymerization kinetics. Further, the model was extended to predict how polymerization conditions, monomer chemistry, and variations in the solvent concentration present during polymerization affect the theoretical mass loss profiles. Finally, the ability of the model to explore how difficult-to-measure network parameters are influenced by numerous variables is highlighted.

## Experimental Section

**PEG-*b*-PLA Diacrylate.** The diacrylated PEG–PLA macromer (PEG<sub>2000</sub>PLA<sub>4</sub>diacrylate, Figure 1a) was prepared using techniques similar to those described by Sawhney et al.<sup>34</sup> and others.<sup>22–24,30</sup> The chemicals used to synthesize this macromer include PEG,  $\bar{M}_n$  2000 Da (PEG<sub>2000</sub>, Aldrich), stannous 2-ethylhexanoate (Sigma), DL-lactide (Polysciences), acryloyl chloride (Fluka), triethylamine (Fisher Scientific), and methylene chloride (Fisher Scientific). Following synthesis, the macromer was purified via vacuum filtration to remove the majority of the triethylamine–hydrochloride salts. To remove the remaining salts, rotary evaporation was used to remove the methylene chloride, the macromer mixture was dissolved in benzene (Fisher Scientific), and the solution was again vacuum filtered. The filtrate was precipitated into a 10:1 excess of iced ethyl ether (Fisher Scientific). All reagents were used as received with the exception of methylene chloride, which was dried with sodium sulfate (Fisher Scientific), vacuum filtered, and stored over molecular sieves (Mallinckrodt). The final product was analyzed by <sup>1</sup>H NMR using a 500 MHz Inova by Varian and was shown to be at least 85% acrylated. The following data was obtained by the <sup>1</sup>H NMR analysis (CDCl<sub>3</sub>): 1.55 ppm (33.86 H, PLA–O–CO–CH–CH<sub>3</sub>–), 3.65 ppm (176.44 H, PEG–O–CH<sub>2</sub>–CH<sub>2</sub>–), 4.27 ppm (4.00 H, last H's on PEG next to PLA block), 5.17 ppm (10.42 H, PLA–O–CO–CH–CH<sub>3</sub>–), 5.9 ppm (dd, 1.59 H, –COO–CH=CH<sub>2</sub>), 6.17 ppm (q, 1.55 H, –COO–CH=CH<sub>2</sub>), 6.47 ppm (dd, 1.61 H, –COO–CH=CH<sub>2</sub>).

**Thiol–Acrylate Monomer Mixture Preparation.** Samples were prepared by mixing together the degradable acrylate macromer with

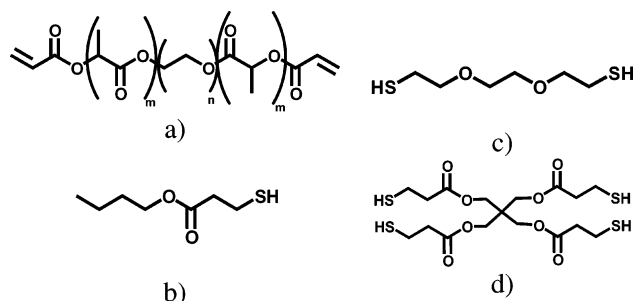


**Figure 1.** (a) PEG<sub>2000</sub>PLA<sub>4</sub>diacrylate ABA triblock macromer with a PEG core ( $n = 45$ ), degradable PLA ( $m = 3–4$ ), and photopolymerizable acrylate endgroups; (b) butyl 3-mercaptopropionate (monothiol); (c) 2,2'-(ethylenedioxy)diethanethiol (dithiol); (d) pentaerythritol tetrakis(3-mercaptopropionate) (tetrathiol).

various thiol monomers (0, 10, 30, and 50 mol % thiol functional groups) and 0.1 wt % 1-[4-(2-hydroxyethoxy)-phenyl]-2-hydroxy-2-methyl-1-propane-1-one (Irgacure 2959, I2959, Ciba) using a procedure previously described.<sup>30</sup> Monofunctional (butyl 3-mercaptopropionate, Figure 1b), difunctional (2,2'-(ethylenedioxy)diethanethiol, Figure 1c), and tetrafunctional (pentaerythritol tetrakis(3-mercaptopropionate), Figure 1d) thiol monomers were used (Aldrich).

**Mid-IR Polymerization Characterization.** To observe real-time polymerization kinetics of thin-film samples, Fourier transform infrared (FTIR) studies were completed using a Nicolet 760 Magna FTIR spectrometer with a KBr beam splitter and MCT/B detector. Monomer mixtures were prepared using the method described above, and a drop of each type was sandwiched between two NaCl crystals. A custom-made temperature cell<sup>35</sup> was used to maintain the sample temperature at 40 °C. Samples were irradiated with 5 mW/cm<sup>2</sup> of 320–500 nm light (peak light intensity at 365 nm, Ultracure, EXFO). In situ observations of polymerization behavior during irradiation were obtained using a horizontal transmission apparatus<sup>36</sup> and the series feature of the Omnic FTIR software that obtained spectra at a rate of 0.67 scans per second. Acrylate conversion was monitored using both the carbon–carbon double-bond absorption double peak at 1636 and 1620 cm<sup>−1</sup> and the out of plane stretch at 810 cm<sup>−1</sup>. The thiol conversion was observed by measuring the area of the S–H absorption peak at 2560 cm<sup>−1</sup>. Conversions were calculated using the ratio of the peak area as a function of time to the peak area prior to irradiation.

**Degradation of Thiol–Acrylate Networks.** Disks were made from the various thiol–acrylate monomer mixtures using the following method: Equal parts of the monomer mixture and dimethyl sulfoxide (DMSO, Fisher Scientific) were mixed in a disposable glass vial, the solution was pipetted into disk-shaped silicon rubber molds that were 10 mm in diameter and 0.9 mm thick. The molds were sandwiched between two glass slides and exposed to 3.5 mW/cm<sup>2</sup> of 365 nm light for 10 min. The disks' initial masses were recorded, samples were placed into labeled tissue cassettes, and cassettes containing the same type of disk were submerged in jars of pH 7.4 phosphate buffer solution. The jars were then placed in an incubated orbital shaker (37 °C, 60 rpm). At specified time points, disks were removed in triplicate, their wet mass measured, and they were lyophilized (Freezone 4.5, Labconco) to obtain their dry mass.

Hydrogel networks are often formed in the presence of solvent, usually water. Here, DMSO was used as the solvent during network formation because of the excellent solubility of both the thiol and the acrylate monomers in DMSO. The concentration of DMSO led to swollen, but not phase separated, gels. All of the swelling and mass loss data reported herein were computed using calculated initial dry masses for each cross-linked polymer disk. These initial dry masses were approximated from the initial DMSO-swollen mass of each disk and the average sol fraction and initial DMSO weight percentages for each network formulation. To calculate the initial sol fractions and dry polymer weight fractions, four disks of each type were weighed (1) right after polymerization, (2) after the DMSO was removed via

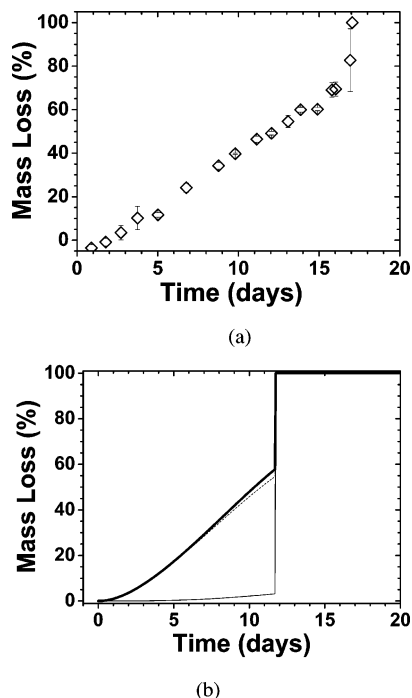


**Figure 2.** (a) Experimentally measured mass loss as a function of degradation time for a thiol–acrylate network formed from a 50 wt % monomer mixture (70 mol % acrylate functional groups, 30 mol % thiol functional groups from the tetrathiol) in DMSO. Polymer specimens were degraded in pH 7.4 PBS on an incubated orbital shaker at 37 °C and 60 rpm. (b) Predicted mass loss behavior for the same network broken down into mass lost from the PEG segments (dashed line), mass lost from the backbone chains (thin solid line), and the total mass lost from the network (thick solid line).<sup>31</sup>

lyophilization, and (3) after the disks were swollen in deionized water for more than 24 h to remove the sol and rehydrophilized. The calculated dry mass values were combined with the temporal wet and dry mass data for each disk to calculate the mass swelling ratio,  $q$ , and the mass loss data.<sup>37</sup> The buffer solution was changed within the first 24 h to remove the DMSO from the systems and then every 3–7 days throughout the duration of this study to maintain sink conditions.

## Results and Discussion

Degradable hydrogels were formed from the photopolymerization of multifunctional thiol and acrylate monomers. This work aims to explore experimentally how changes in thiol group concentration and thiol monomer functionality impact mass loss behavior. That understanding of the relationship between network structure and mass loss behavior is then extended to predict the impact of variations in solvent concentration, monomer chemistry, and polymerization conditions on mass loss behavior.

**Thiol–Acrylate Mass Loss Behavior.** Degradable thiol–acrylate photopolymers typically exhibit mass loss throughout all stages of degradation. This mass loss continues in a nearly linear fashion until a sufficient fraction of the cross-links have degraded such that an infinite molecular weight gel no longer exists, and the mass loss increases sharply as the network undergoes rapid dissolution at the “reverse gelation point.” The data in Figure 2a display this increase in mass loss with increasing degradation time for a thiol–acrylate network synthesized from a monomer solution containing 70 mol % acrylate and 30 mol % thiol functional groups. The observed mass loss profile is correlated to the release of three primary degradation products: PEG, thiol–polyacrylate backbone chains,

and backbone chains with dangling PLA-*b*-PEG segments still attached. Reverse gelation is observed in this network after approximately 17 days.

Figure 2b presents the model predictions of the mass loss profile for this network. The simulated results follow the trends in the mass loss behavior observed experimentally in Figure 2a, and provide further insight by separating the mass loss into the fractional portions related to the PEG and the thiol–polyacrylate backbones. From this analysis, one observes that the initial mass loss is primarily PEG. Only after ~30% mass loss is the contribution from the thiol–polyacrylate chains detectable, and even then it is a small contribution. For this system, where 92% of the network’s mass is located in the PEG portions of the cross-links, the small contribution to the mass loss profile from the thiol–polyacrylate chains is not surprising. Additionally, the model predictions shown in Figure 2b predict that reverse gelation occurs at approximately 12 days when 60% of the initial mass has been eroded, which is different than what was observed experimentally. This discrepancy is most likely due to differences in the number of cross-links connecting each backbone chain between the model and the actual networks. The actual number of cross-links could be approximated analytically from gel permeation chromatograms of the backbone chains. Alternatively, delayed dissolution of the highly branched backbone chains may allow masses to be measured after reverse gelation has occurred, making the reverse gel point seem later experimentally than it actually is.

The thiol–acrylate mass loss profiles exhibit three stages of degradation. During the first stage, the PEG cores from each PEG diacrylate are released since they are connected to the network by two PLA segments. This connectivity leads to nearly identical initial mass loss profiles for networks that have similar PEG weight fractions. As more PLA groups cleave, the network transitions into the second stage of degradation where the backbone chains and their dangling PLA-*b*-PEG segments begin to be released. The transition to this second stage of degradation strongly depends on the distribution of thiol–polyacrylate backbone chain lengths. The final stage of degradation, where reverse gelation occurs, is also highly dependent on the distribution of backbone chain lengths since reverse gelation depends on the number of cross-links connecting each backbone to the rest of the network. Finally, the temporal duration of each of the observed mass loss stages depends on the polymer network structure and on the kinetic rate constant for the ester hydrolysis.

For the thiol–acrylate networks investigated in this research, the hydrolysis rate constant ( $k_{\text{hyd}}$ ) and the backbone chain length distribution are both impacted by variations in thiol monomer functionalities and relative thiol functional group concentrations. A theoretical model originally developed by Metters et al.<sup>23</sup> and amended by Reddy et al.<sup>31</sup> enables the impact of these two parameters to be explored independently.

**Predicting Thiol–Acrylate Mass Loss Profiles.** The thiol–acrylate mass loss model<sup>31</sup> is based on three main equations. The first equation accounts for the mass lost due to the release of the backbone chains and the PEG cores of each cross-link (eq 1), each being the combination of their mass fraction in the network ( $W$ ) and their probability of being released ( $F$ ) at a specific extent of degradation ( $P$ ). The other two equations describe the probability of PEG (eq 2) and the thiol–polyacrylate chains (eq 3) eroding from the network at a particular extent of degradation. The probability that any random degradable block has cleaved,  $P$ , and the weighted fraction of backbone chains of length  $i$  ( $w_i$ ) are shown in eqs 4 and 5, respectively,

where  $j$  is the number of lactic acid repeat units per PLA segment,  $k_{\text{hyd}}$  is the pseudo first-order reaction constant of ester hydrolysis, and  $A_i$  is the fraction of thiol–acrylate backbone chains that have  $N_i$  cross-links originally attached to them.  $A_i$  accounts for the thiol monomer functionality, the initial thiol functional group concentration, the extent of thiol and acrylate conversion, and the relative consumption of thiol and acrylate functional groups during polymerization. A detailed description of the dependence of  $A_i$  on each of these factors has been presented previously.<sup>31</sup>

$$\% \text{ mass loss} = (W_{\text{kc}}F_{\text{kc}} + W_{\text{PEG}}F_{\text{PEG}}) \quad (1)$$

$$F_{\text{PEG}} = P^2 + F_{\text{kc}}(P(1 - P)) \quad (2)$$

$$F_{\text{kc}} = \sum_i w_i [1 - (1 - P)^2]^{N_i} \quad (3)$$

$$P = 1 - e^{-jk_{\text{hyd}}t} \quad (4)$$

$$w_i = \frac{A_i N_i}{\sum A_i N_i} \quad (5)$$

The main deviation from this model and the one that was originally developed to predict mass loss in acrylate chain growth networks<sup>23</sup> is the modification of eq 3 that replaces the average number of acrylates reacted into each backbone chain ( $N_{\text{avg}}$ ) with the distribution of the thiol–polyacrylate backbone chains ( $w_i$  and  $N_i$ ). In essence, this change allows the fraction of released thiol–polyacrylate chains ( $F_{\text{kc}}$ ) to account for both the extent of degradation ( $P$ ) and the structural variations in network connectivity that arise from the distribution of thiol–polyacrylate chain lengths. This adjustment is important for accurate thiol–acrylate mass loss predictions because the distribution of backbone chain lengths can be broad. Failing to account for variations in chain length within these thiol–acrylate networks underpredicts both the mass loss profiles prior to reverse gelation and the degradation time at which reverse gelation occurs. Adjusting eq 3 to account for the variability in chain length within these networks allows the impact of changes in thiol functionality and stoichiometry on mass loss behavior to be predicted using this model. Additionally, the thiol–acrylate mass loss model accounts for the influence of variations in backbone chain length distributions on reverse gelation (eq 6–7),<sup>31</sup> where  $P_{\text{rev}}$  is the extent of degradation (hydrolysis of PLA segments) at reverse gelation, and  $N_{\text{avg}}$  is the weight-average number of acrylates reacted to each thiol monomer.

$$P_{\text{rev}} = 1 - \frac{1}{\sqrt{N_{\text{avg}} - 1}} \quad (6)$$

$$N_{\text{avg}} = \frac{\sum A_i N_i^2}{\sum A_i N_i} \quad (7)$$

**Probing How Variations in  $k_{\text{hyd}}$  and Chain Length Distribution Impact Thiol–Acrylate Mass Loss.** A significant advantage of theoretically predicted mass loss profiles is the ability to rapidly and independently probe how various model parameters impact network structure and mass loss profile. The influence of  $k_{\text{hyd}}$  and the backbone chain length distribution, two key parameters impacting thiol–acrylate mass loss behavior, are discussed below.

Mass loss profiles were predicted for four different rates of PLA hydrolysis ( $k_{\text{hyd}}$ , Figure 3). The data in this figure indicate

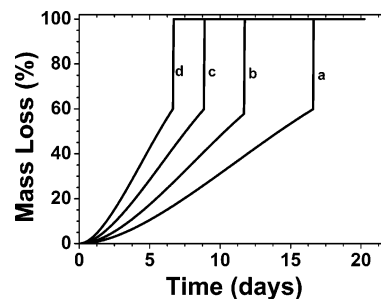


**Figure 3.** Impact of  $k_{\text{hyd}}$  on thiol–acrylate mass loss profiles. Mass loss profiles are predicted for thiol–acrylate networks made from monomer mixtures containing 30 mol % thiol functional groups (from the tetrathiol) with  $k_{\text{hyd}}$  values of (a) 0.08, (b) 0.11, (c) 0.15, and (d) 0.20 days<sup>-1</sup>.

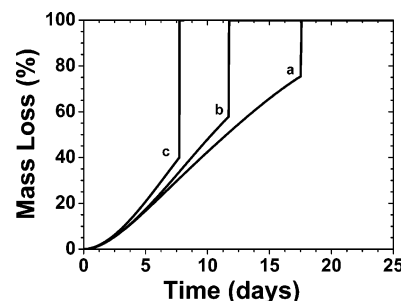


**Figure 4.** Impact of the backbone chain length distribution on thiol–acrylate mass loss profiles. Mass loss profiles are predicted for thiol–acrylate networks made from monomer mixtures containing (a) 10 ( $N_{\text{avg}} = 47$ ), (b) 30 ( $N_{\text{avg}} = 13$ ), and (c) 50 ( $N_{\text{avg}} = 7$ ) mol % thiol functional groups.  $W_{\text{PEG}} = 0.90$ ,  $k_{\text{hyd}} = 0.11$  days<sup>-1</sup>, thiol functionality = 4, and  $k_{p,c-d}/k_{CT} = 2.04$ .

that increasing  $k_{\text{hyd}}$  increases the slope of the mass loss curve and reduces the degradation time required to achieve reverse gelation. Increasing  $k_{\text{hyd}}$  does not, however, change the percent mass loss at which reverse gelation occurs. If the data in Figure 3 were plotted as a function of the extent of degradation,  $P$ , instead of as a function of degradation time, all four lines would collapse onto one another.

Figure 4 demonstrates the predicted change in mass loss profiles as the backbone chain length distribution is varied for networks synthesized from monomer solutions containing 10, 30, and 50 mol % thiol functional groups that originated from a tetrafunctional thiol monomer. In these networks, decreasing the ratio of thiol functional groups shifts the chain length distribution toward higher molecular weight backbone chains, increasing the number of cross-links connecting each thiol–polyacrylate chain to the rest of the network ( $N_{\text{avg}}$ ). Observing the data in Figure 4 reveals that this increase in  $N_{\text{avg}}$  delays the degradation time and the mass loss percent at which reverse gelation occurs. The slope of the mass loss curves at early degradation times is not altered by this change in  $N_{\text{avg}}$ , but, at later degradation times, increasing  $N_{\text{avg}}$  slightly decreases the slope of the mass loss profiles.

Shifting the chain length distribution toward longer thiol–polyacrylate chains increases the extent of degradation,  $P$ , required for these thiol–polyacrylate chains to be released from the network, which is what is responsible for the shift in reverse gelation to later degradation times and higher mass loss percentages. Additionally, this thiol–acrylate mass loss model accounts for the distribution of backbone chains, not just  $N_{\text{avg}}$ . Because a decrease in the ratio of thiol functional groups increases the number of high molecular weight chains and broadens the chain length distribution, the fraction of thiol–polyacrylate chains that are released at higher  $P$  is dramatically

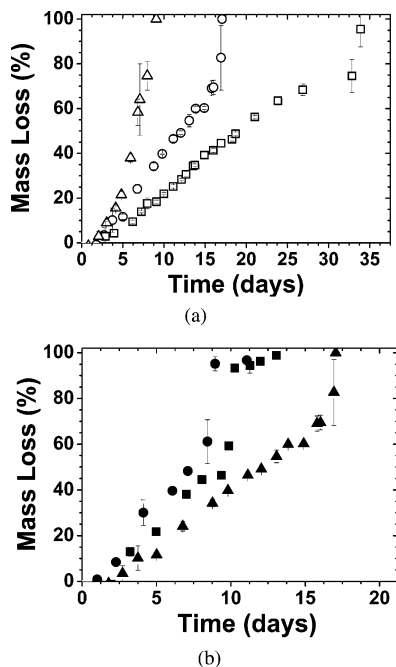


**Figure 5.** Experimental mass loss profiles for degradable thiol–acrylate networks made from a PEG–PLA diacrylate and (a) 10 (□), 30 (○), and 50 (Δ) mol % thiol functional groups originating from a tetrathiol monomer or (b) 30 mol % thiol functional groups originating from mono- (■), di- (●), and tetrafunctional (▲) thiol monomers.

decreased. The impact of this effect on the mass loss profiles in Figure 4 is diminished only because  $W_{kc}$  is 0.1.

**Influence of Thiol Functional Group Concentration and Thiol Monomer Functionality on Mass Loss Profiles: Experimental Observations.** Figure 5 plots the mass loss percentages as a function of degradation time for thiol–acrylate networks synthesized from monomer solutions containing different thiol functional group concentrations and different thiol monomer functionalities. The data in Figure 5a exhibit an increase in the mass loss rate and a decrease in the degradation time and the extent of mass loss at reverse gelation as thiol concentrations were increased. In Figure 5b, increasing thiol monomer functionality from 1 to 4 decreased the mass loss rate and increased the degradation time and extent of mass loss at reverse gelation. Networks made from the dithiol exhibited different behavior, likely due to the differences in chemical reactivity between the various types of thiols, which will also influence the thiol–polyacrylate chain length distribution.

**Determining  $k_{hyd}$  from Changes in Equilibrium Swelling Ratios.** To predict the mass loss profiles exhibited in Figure 5,  $k_{hyd}$  values were determined from changes in the experimental equilibrium swelling ratios using a method similar to the one first described by Metters et al. for highly swollen gels.<sup>23</sup> Briefly, equilibrium swelling ratios in degrading networks increase exponentially as a function of degradation time. The network cross-linking density, in turn, decreases exponentially as esters within the PLA segments hydrolyze. When a simplified version of the Flory–Rehner equation<sup>38</sup> for highly swollen gels is further simplified by assuming that the average molecular weight between cross-links and  $\chi_{12}$ , the Flory interaction parameter, do not change significantly throughout the early stages of network degradation, changes in the volume equilibrium swelling ratio,  $Q$ , are proportional to changes in  $\rho_x^{-3/5}$  (eq 8). Equation 9 relates the cross-linking density to the extent of ester hydrolysis while accounting for the triblock structure of the PLA-*b*-PEG-*b*-PLA cross-link chemistry. Coupling this exponential decay of the network’s cross-linking density with the

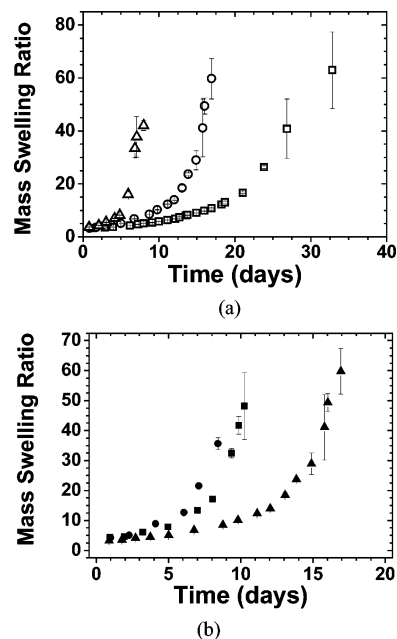


**Figure 6.** Mass equilibrium swelling ratios for (a) 10 (□), 30 (○), and 50 (Δ) mol % tetrathiol or (b) 30 mol % mono- (■), di- (●), and tetrafunctional (▲).

experimentally observed exponential increase in the equilibrium swelling ratio allows  $k_{hyd}$  to be calculated from eq 10, where  $Q_0$  is the initial volume equilibrium swelling ratio, and  $\tau_Q$  is the experimentally determined rate constant for the exponential increase in swelling.<sup>23</sup>

$$Q = \left[ \frac{1}{V_1} \left( \frac{1}{1 - \frac{2\bar{M}_c}{\bar{M}_n}} \right) \left( \frac{1}{2} - 2\chi_{12} \right) \right]^{3/5} \rho_x^{-3/5} \therefore Q \propto \rho_x^{-3/5} \quad (8)$$

$$\rho_x \approx (1 - P)^2 = e^{-2jk_{hyd}t} \quad (9)$$

$$Q = Q_0 e^{\tau_Q t} \therefore k_{hyd} = \frac{-5}{6} \frac{\tau_Q}{j} \quad (10)$$

Figure 6 plots the mass equilibrium swelling ratios ( $q$ ) as a function of degradation time for the same thiol–acrylate networks from Figure 5. For the samples studied here,  $Q$  and  $q$  are very similar since the polymer and solvent densities are near 1. Figure 6a documents how the swelling ratio changes for networks made with varying amounts of a tetrathiol monomer. The initial values ( $q_0$ ) for the data in this figure are highest for the 50 mol % networks ( $3.7 \pm 0.03$ ) and decrease slightly for the 30 and 10 mol % networks ( $3.3 \pm 0.05$  and  $3.2 \pm 0.2$ , respectively, which are not significantly different at the 95% confidence interval). As the cross-links degrade, the mass equilibrium swelling ratio increases with increasing degradation time in each type of network. The rate at which  $q$  increases is accelerated for networks synthesized from monomer solutions with higher thiol functional group ratios, which leads to an increase in the  $k_{hyd}$  values. The  $k_{hyd}$  values that were determined from experimental fits of the swelling data shown in Figure 6a are presented in Table 1.

Figure 6b tracks changes in  $q$  for networks made from 30 mol % thiol functional groups where the thiol monomer functionality ranged from 1 to 4. Increasing the thiol monomer functionality from 1 to 4 slightly increased the initial equilibrium swelling ratio from  $3.3 \pm 0.05$  to  $4.3 \pm 0.02$ . As these two networks start to degrade, the rate at which  $q$  increases is

**Table 1.**  $k_{\text{hyd}}$  Values for the Various Thiol–Acrylate Networks Calculated from the Exponential Increase in Equilibrium Swelling Ratios with Degradation Time

functional group concentration (mol %)	thiol monomer functionality	$k_{\text{hyd}}$ (days <sup>-1</sup> )
10	4	0.067 ± 0.002
30	4	0.11 ± 0.003
50	4	0.17 ± 0.02
30	1	0.13 ± 0.02
30	2	0.19 ± 0.02

accelerated for the monothiol-containing polymer, leading to a larger hydrolysis kinetic constant for the monothiol materials. The initial swelling ratio for the dithiol networks was not statistically different from the  $q_0$  values of the monothiol networks at  $4.2 \pm 0.1$ , but the rate at which  $q$  increased as degradation commenced was greatest for the dithiol sample set. As a result, the dithiol samples exhibited the largest  $k_{\text{hyd}}$  values for the different monomer functionalities. The  $k_{\text{hyd}}$  values that were determined from experimental fits of the data in Figure 6b are presented in Table 1.

While the mechanisms responsible for the observed increase in  $k_{\text{hyd}}$  values with increasing thiol concentration and when thiol functionality was changed from 4 to 1 to 2 are not completely understood, similar behavior was previously observed for PEG-based polyacrylate chain growth networks.<sup>36</sup> For the networks formed from chain growth reactions, Metters and co-workers observed an acceleration in the degradation kinetics when the solvent concentration present during network formation was increased. They attributed these observations to increases in equilibrium swelling ratios and water concentrations in the hydrogels with increasing initial solvent concentration. A similar dependence of swelling behavior and  $k_{\text{hyd}}$  are observed for the thiol–acrylates investigated here (Figure 6 and Table 1), where solvent concentrations were held constant and thiol functional group concentration or thiol monomer functionality were varied.

**Predicting the Length Distribution of the Thiol–Polyacrylate Backbone Chains.** A key component of the thiol–acrylate mass loss model is an understanding of the distribution of the thiol–polyacrylate backbone chain lengths. Theoretically predicted chain length distributions<sup>31</sup> were utilized to predict the thiol–acrylate mass loss profiles shown in Figure 5. A central component of the chain length distribution predictions is the probability that an acrylic radical homopolymerizes ( $p_h$ , eq 11), relative to all other possible propagation reactions. The probability of forming a thiol–polyacrylate chain of length  $n$  requires acrylate homopolymerization to happen  $n - 1$  times and chain transfer with thiol ( $1 - p_h$ ) to happen once (eq 12). Equation 12 predicts the average number of acrylate groups that react per thiol group at a given extent of thiol–acrylate conversion, but the relative functional group ratio changes throughout the polymerization, requiring the summation of the  $p(n)$ 's at each conversion to determine the overall distribution of polyacrylate chain lengths. The distribution of the number of acrylate groups attached to multifunctional thiol monomers was determined by statistically averaging the distribution of the individual polyacrylate chains on each arm of the thiol monomer.<sup>31</sup>

$$p_h = \frac{k_{p,c=c}[C=C]}{k_{p,c=c}[C=C] + k_{CT}[SH]} \quad (11)$$

$$p(n) = p_h^{n-1}(1 - p_h) \quad (12)$$

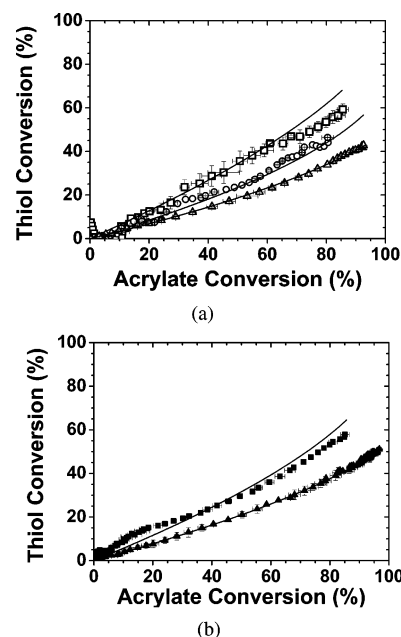


**Figure 7.** Plots of thiol functional group conversion as a function of acrylate group conversion used to determine  $k_{p,c=c}/k_{CT}$  for (a) 10 (□), 30 (○), and 50 (△) mol % thiol functional groups from the tetrathiol monomer and (b) 10 (■) and 50 (▲) mol % thiol functional groups from the dithiol. The  $k_{p,c=c}/k_{CT}$  ratios were determined through regression analysis that minimized the error between the experimental (symbols) and theoretical (lines) 50 mol % data.

The distribution of backbone chain lengths is influenced by functional group concentrations, monomer functionality, and  $k_{p,c=c}/k_{CT}$  ratios. Independently monitoring the conversion of the thiol and acrylate functional groups during photopolymerization using real-time FTIR spectroscopy allows the  $k_{p,c=c}/k_{CT}$  ratios to be determined for the different thiol monomers as described elsewhere.<sup>32</sup> Figure 7 shows a plot of thiol conversion as a function of acrylate conversion. The  $k_{p,c=c}/k_{CT}$  ratios determined using this method for the tetrathiol and dithiol monomers are 2.0 and 1.7, respectively. These values are of the same order as those reported in the literature for nondegradable polymers.<sup>32,39</sup>

Interestingly, the  $k_{p,c=c}/k_{CT}$  ratio for the dithiol is less than that for the tetrathiol and monothiol monomers (monothiol data not shown). This difference in polymerization behavior is most likely due to differences in thiol monomer chemistry which makes the dithiol monomer more likely to undergo chain transfer (step 3) than the mono- or tetrathiol monomers, thereby reducing the  $k_{p,c=c}/k_{CT}$  ratio. At a given conversion and initial concentration of thiol and acrylate functional groups, larger  $k_{p,c=c}/k_{CT}$  ratios result in longer backbone chains being formed, directly impacting the network structure in these cross-linked polymeric materials.

Using the  $k_{p,c=c}/k_{CT}$  values determined from Figure 7, the backbone chain length distributions were predicted for each of the different thiol–acrylate networks in this study. The chain length distribution predictions in Figure 8a for the networks with varying thiol concentrations show that increasing the thiol concentration narrows the distribution of backbone chain lengths and shifts the distribution toward lower molecular weight chains. The data in Figure 8b for networks fabricated from thiols of different functionalities indicates that increasing thiol functionality broadens the chain length distribution while shifting the distribution toward higher molecular weight chains.

**Evaluating the Thiol–Acrylate Mass Loss Model's Performance.** Figure 9 plots the experimentally observed and theoretically predicted mass loss curves for the various networks

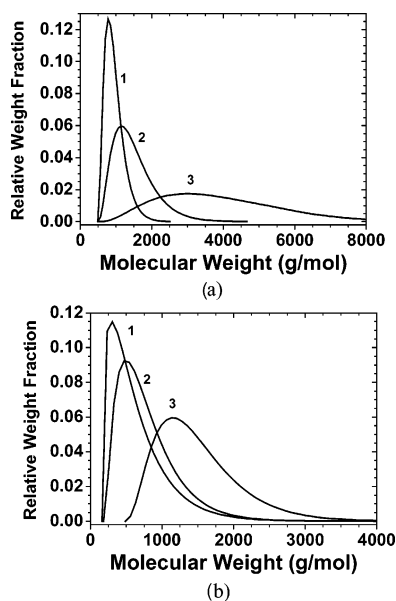


**Figure 8.** Predicted distributions of the backbone chains in thiol–acrylate networks made from degradable diacrylates and (a) 50 (1), 30 (2), and 10 (3) mol % thiol functional groups from the tetrathiol or (b) 30 mol % thiol functional groups from mono- (1), di- (2), and tetrathiol (3).

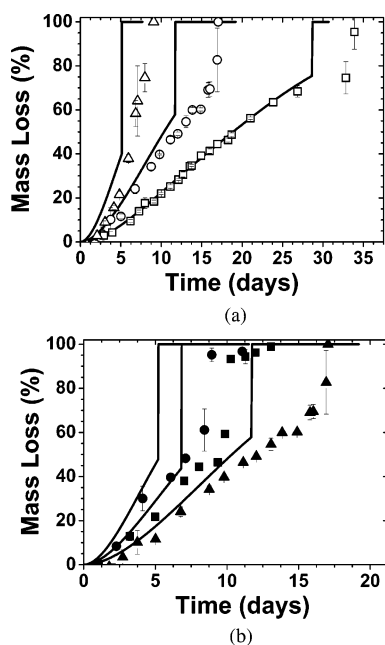


**Figure 9.** Comparison of theoretical (lines) and experimental (symbols) mass loss profiles for degradable thiol–acrylate networks made from a PEG–PLA diacrylate and (a) 10 (□), 30 (○), and 50 (△) mol % tetrathiol or (b) 30 mol % mono- (■), di- (●), and tetrathiol (▲).

investigated in this study. In general, the thiol–acrylate mass loss model captures the general trends observed for the experimental data. Increasing the ratio of thiol functional groups or decreasing thiol monomer functionality decreases the degradation time and mass loss percentage where reverse gelation occurs, with the exception of the dithiol data. Closer inspection of the data reveals that, while the model and experimental data are in excellent agreement for the networks made with 10 mol % tetrathiol, for all other networks, the model predicts more rapid degradation behavior than that experimentally observed. Reverse gelation is also predicted to occur at earlier degradation times and lower mass loss percentages than what is observed experimentally.

**Table 2.**  $k_{\text{hyd}}$  Values for the Various Thiol–Acrylate Networks Calculated from Regression Analysis of the Mass Loss Data

functional group concentration (mol %)	thiol monomer functionality	$k_{\text{hyd}}$ (days <sup>-1</sup> )	
		swelling	mass loss
10	4	0.067	0.065
30	4	0.11	0.092
50	4	0.17	0.12
30	1	0.13	0.09
30	2	0.19	0.14

While the underlying causes responsible for these observed deviations are not known, the information obtained from Figure 3 and Figure 4 about the mass loss model's predictive abilities permit a few conclusions to be drawn. For example, the  $k_{\text{hyd}}$  values determined from equilibrium swelling data are too large to capture the experimental mass loss profiles accurately, causing the model to overpredict mass loss for most of the data in Figure 9. Regression analysis was used to determine hydrolysis kinetic constants directly from the mass loss data. These new  $k_{\text{hyd}}$  values, shown in Table 2, are all smaller than the original values listed in Table 1 but are generally consistent within one significant figure. Additionally, the discrepancy between the model and experimental data with respect to the reverse gelation point may be due to difficulties in obtaining accurate experimental mass loss measurements at very high extents of degradation.

**Predicting Mass Loss Profiles for other Networks Formed through Mixed-Mode Polymerizations.** Variations in thiol monomer functionality and thiol functional group concentration are only two of the means by which the network structure and mass loss profiles are altered. Changing solvent concentration, monomer chemistry, and polymerization conditions are other examples of pathways through which mass loss profiles are changed and biomaterials with specific characteristics designed. The thiol–acrylate mass loss model is a useful tool for this design process, because it allows the impact of these various parameters on the mass loss profile to be approximated quickly.

Others have shown that, as the solvent concentration present during polymerization increases in networks formed from acrylate chain growth reactions, the fraction of diacrylates that form primary cycles ( $f_c$ ) also increases.<sup>40</sup> The thiol–acrylate mass loss model initially neglects the presence of primary cycles and assumes that all of the acrylate groups that polymerize react into separate chains, each acting as a cross-link. Figure 10a plots predictions of the fraction of reacted acrylate monomers that form primary cycles ( $f_c$ ) as a function of the thiol functional group ratio for two different solvent concentrations. The predictions shown in this plot indicate that increasing the solvent concentration or decreasing the thiol functional group concentration both increase the extent of cyclization. Figure 10b compares the original mass loss predictions ( $f_c = 0$ ) to modified mass loss predictions that incorporate the  $f_c$  values<sup>22</sup> predicted for networks synthesized from monomer solutions that contain 50 wt % solvent. Clearly, as  $f_c$  increases, the degradation rate is accelerated and is indicative of increased cyclization.

The impact of changing monomer chemistry on the mass loss behavior is demonstrated by the dithiol sample in Figure 5b. For the three samples in this figure, one would expect the time required to reach reverse gelation to increase with monomer functionality. Instead, the dithiol sample is the first to fully degrade. Closer inspection reveals that while the mono- and tetrathiol monomers have the same core chemistry, the dithiol monomer's chemistry is quite different. As a result, the dithiol's  $k_{\text{hyd}}$  is increased to the extent that the observed mass loss

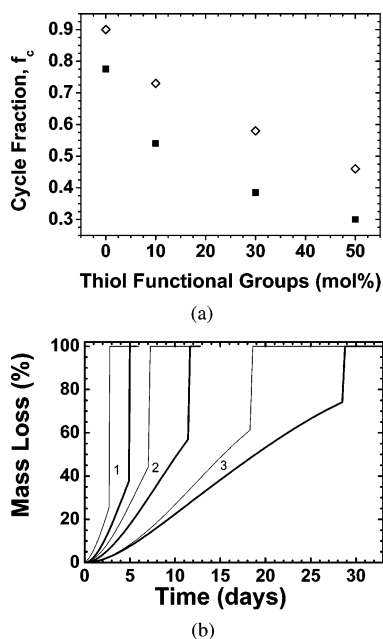


**Figure 10.** The fraction of acrylate functional groups that form primary cycles ( $f_c$ ) and their influence on the predicted mass loss profile for a thiol–acrylate network containing 30 mol % tetrathiol: (a) predicted cycle fraction,  $f_c$ , for no solvent (filled symbols) and 50 wt % solvent (open symbols) and (b) predicted mass loss profiles neglecting  $f_c$  (thick line) and accounting for the  $f_c$  values (thin line) that occur in the presence of 50 wt % solvent for networks made from (1) 50, (2) 30, and (3) 10 mol % thiol functional groups.

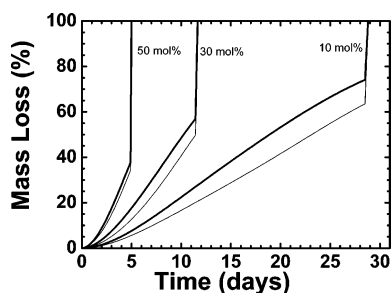


**Figure 11.** Theoretical model predictions of the influence of the weight fraction of PEG and backbone chains ( $W_{PEG}$  and  $W_{kc}$ ) in the network on thiol–acrylate mass loss behavior for networks made from 50, 30, and 10 mol % thiol functional groups using a tetrafunctional thiol monomer. The  $W_{PEG}$  and  $W_{kc}$  values are shown in Table 3. The thicker lines represent the original predictions, the thinner lines account for a 5-fold increase in  $W_{kc}$ .

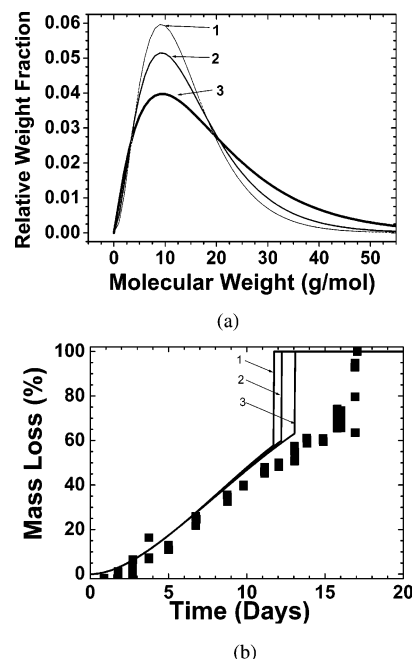
behavior deviates from what would be expected for a monomer with the same core chemistry as the mono- and tetrathiol monomers. Similarly, changes in monomer chemistry that impact the degradable portions of the cross-links in the polymerized networks will impact mass loss behavior by altering  $k_{hyd}$ .

Figure 11 demonstrates how changes in monomer chemistry influence mass loss behavior. The simulated results presented in this figure illustrate how a 5-fold increase in the weight fraction of the network that is coming from the backbone chains ( $W_{kc}$ ) dramatically affects the extent of mass loss at reverse gelation without changing the time at which reverse gelation occurs. The  $W_{kc}$  and  $W_{PEG}$  values used to calculate the curves in this figure are listed in Table 3. Both  $W_{kc}$  and  $W_{PEG}$  are easily adjusted through manipulations in the monomer's molecular weights and functional group ratios.

Figure 12 investigates how variations in monomer chemistry impact the ratio of propagation events to chain transfer events

**Table 3.** The Original and Modified Values of  $W_{PEG}$  and  $W_{kc}$  Used to Predict the Mass Loss Profiles Shown in Figure 11

	50 mol %	30 mol %	10 mol %
$W_{kc}$ original	0.121	0.083	0.061
$W_{PEG}$ original	0.879	0.917	0.939
$5 \times W_{kc}$	0.607	0.415	0.307
$0.2 \times W_{PEG}$	0.393	0.585	0.693



**Figure 12.** Theoretical predictions of the influence of  $k_{p,c} = \alpha/k_{CT}$  on (a) chain length distribution and (b) thiol–acrylate mass loss. 30 mol % tetrathiol,  $k_{p,c} = \alpha/k_{CT} =$  (1) 2.0 (used for original mass loss predictions), (2) 2.5, and (3) 4; experimental mass loss data (■) shown for comparison in panel b.

( $k_{p,c} = \alpha/k_{CT}$ ) during photopolymerization. Part a of this figure demonstrates how increasing  $k_{p,c} = \alpha/k_{CT}$  broadens the distribution of chain lengths and shifts the distribution toward a higher average number of acrylates attached per reacted thiol group. The chain length distribution changes primarily by increasing the area of the peak's tail that represents the highest molecular weight chains. Part b of this figure uses the distributions of the backbone chain lengths shown in part a to predict how these variations in network structure impact the mass loss profiles. These results indicate that increasing the  $k_{p,c} = \alpha/k_{CT}$  ratio does not significantly alter the early mass loss kinetics, but it does shift the percent mass loss and time where reverse gelation occurs to higher values. For the various thiol monomer functionalities and thiol functional group concentrations explored in this study, this shift is most apparent for samples with distributions of shorter chain lengths (e.g., higher concentration of thiol functional groups or lower thiol monomer functionality).

In addition to predicting how numerous parameters impact thiol–acrylate mass loss profiles, the model is a useful tool for determining how these parameters impact other network properties that are often hard to measure experimentally. Figure 13 highlights the usefulness of the model for predicting the impact of multiple network variables on several difficult-to-characterize aspects of degradation by calculating the fraction of the total mass loss that is associated with the PEG portions of the material. The particular example highlighted in Figure 13 explores how two parameters, the thiol functional group concentration and the thiol monomer functionality, impact the fraction of the total mass loss that is being contributed by the

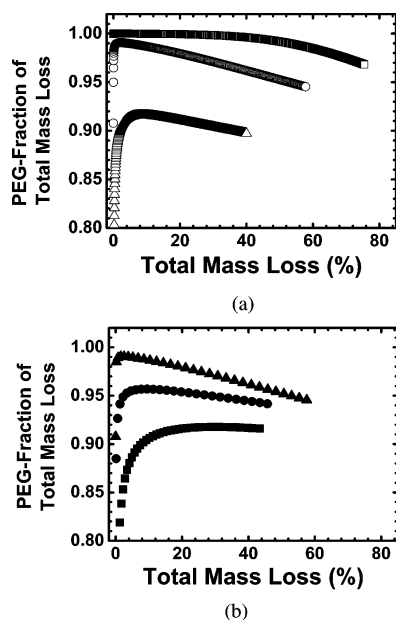


**Figure 13.** Model predictions of the fraction of total mass loss contributed by the PEG portion of each cross-link for networks containing different thiol functional group concentrations (a) and thiol monomers having different functionalities (b). In panel a, the various polymer networks contain 10 ( $\square$ ), 30 ( $\circ$ ), and 50 ( $\triangle$ ) mol % tetrathiol. In panel b, the samples contain 30 mol % mono- ( $\blacksquare$ ), di- ( $\bullet$ ), and tetra- ( $\blacktriangle$ ).

PEG. On the basis of the trends exhibited by the data in this figure, it can be concluded that both increasing the thiol functional group concentration and decreasing the thiol monomer functionality decreases the fraction of the total mass loss that is coming from the PEG. The model is readily extended further to explore the impact of other properties such as (1) the network weight fractions contributed by PEG and the backbone chains, (2) the fraction of the acrylate monomer's chain ends that are functionalized, and (3) the solvent concentration present during polymerization on the fraction of total mass loss that is coming from the PEG.

### Conclusions

The mass loss behavior of degradable thiol–acrylate biomaterials is predictably controlled through variations in monomer functionality, functional group concentration, and monomer core chemistry. A model developed by Reddy et al.<sup>31</sup> is able to predict the mass loss behavior of these networks. Manipulations of the various model parameters identified the backbone chain length distribution and  $k_{\text{hyd}}$  as the most influential factors for these thiol–acrylate networks. Shifting the chain length distributions toward shorter, more monodisperse backbone chains by increasing the relative thiol reactivity or concentration of the thiol functional groups decreases the time and percent mass loss at which reverse gelation occurs, as well as increases the mass loss prior to reverse gelation. Increasing the hydrolysis rate constant significantly influences the slope of the mass loss curve prior to reverse gelation without changing the percent mass loss where reverse gelation occurs. In addition to capturing the mass loss trends exhibited by various thiol–acrylate networks, the model is a useful tool for predicting how numerous variables impact mass loss profiles for these mixed-mode networks.

**Acknowledgment.** The authors thank their funding sources for this work, a grant from the NIH (R01 DE12998), an NSF

Industry/University Cooperative Research Center for Fundamentals and Applications of Photopolymerization and a National Science Foundation Tie Grant (EEC-0120943), and a Department of Education GAANN fellowship and a University of Colorado Beverly Sears Graduate Student Grant to A.E.R.

### References and Notes

- Burdick, J. A.; Anseth, K. S. Photoencapsulation of osteoblasts in injectable RGD-modified PEG hydrogels for bone tissue engineering. *Biomaterials* **2002**, *23* (22), 4315–4323.
- Burdick, J. A.; Mason, M. N.; Anseth, K. S. In situ forming lactic acid based orthopaedic biomaterials: Influence of oligomer chemistry on osteoblast attachment and function. *J. Biomater. Sci., Polym. Ed.* **2001**, *12* (11), 1253–1265.
- Mason, M. N.; Metters, A. T.; Bowman, C. N.; Anseth, K. S. Predicting controlled-release behavior of degradable PLA-*b*-PEG-*b*-PLA hydrogels. *Macromolecules* **2001**, *34* (13), 4630–4635.
- Nuttelman, C. R.; Henry, S. M.; Anseth, K. S. Synthesis and characterization of photocrosslinkable, degradable poly(vinyl alcohol)-based tissue engineering scaffolds. *Biomaterials* **2002**, *23* (17), 3617–3626.
- Nuttelman, C. R.; Tripodi, M. C.; Anseth, K. S. Synthetic hydrogel niches that promote hMSC viability. *Matrix Biol.* **2005**, *24* (3), 208–218.
- Quick, D. J.; Anseth, K. S. Gene delivery in tissue engineering: A photopolymer platform to coencapsulate cells and plasmid DNA. *Pharm. Res.* **2003**, *20* (11), 1730–1737.
- Quick, D. J.; Macdonald, K. K.; Anseth, K. S. Delivering DNA from photocrosslinked, surface eroding polyanhydrides. *J. Controlled Release* **2004**, *97* (2), 333–343.
- Nguyen, K. T.; West, J. L. Photopolymerizable hydrogels for tissue engineering applications. *Biomaterials* **2002**, *23* (22), 4307–4314.
- Hubbell, J. A. Synthetic biodegradable polymers for tissue engineering and drug delivery. *Curr. Opin. Solid State Mater. Sci.* **1998**, *3*, 246–251.
- Langer, R.; Peppas, N. A. Advances in biomaterials, drug delivery, and bionanotechnology. *AIChE J.* **2003**, *49* (12), 2990–3006.
- Anseth, K. S.; Burdick, J. A. New directions in photopolymerizable biomaterials. *MRS Bull.* **2002**, *27* (2), 130–136.
- Anseth, K. S.; Metters, A. T.; Bryant, S. J.; Martens, P. J.; Elisseeff, J. H.; Bowman, C. N. In situ forming degradable networks and their application in tissue engineering and drug delivery. *J. Controlled Release* **2002**, *78* (1–3), 199–209.
- Elbert, D. L.; Hubbell, J. A. Conjugate addition reactions combined with free-radical cross-linking for the design of materials for tissue engineering. *Biomacromolecules* **2001**, *2* (2), 430–441.
- Fisher, J. P.; Holland, T. A.; Dean, D.; Mikos, A. G. Photoinitiated cross-linking of the biodegradable polyester poly(propylene fumarate). Part II. In vitro degradation. *Biomacromolecules* **2003**, *4* (5), 1335–1342.
- Gutowska, A.; Jeong, B.; Jasionowski, M. Injectable gels for tissue engineering. *Anat. Rec.* **2001**, *263* (4), 342–349.
- Pachence, J. M.; Kohn, J. Biodegradable polymers for tissue engineering. In *Principles of Tissue Engineering*; Lanza, R., Langer, R., Chick, W., Eds.; R. G. Landes Company: Austin, TX, 1997.
- Palsson, B. O.; Bhatia, S. N. *Tissue Engineering*; Pearson Prentice Hall: Upper Saddle River, NJ, 2004.
- Seal, B. L.; Otero, T. C.; Pantich, A. Polymeric biomaterials for tissue and organ regeneration. *Mater. Sci. Eng.* **2001**, *34*, 147–230.
- Temenoff, J. S.; Athanasiou, K. A.; LeBaron, R. G.; Mikos, A. G. Effect of poly(ethylene glycol) molecular weight on tensile and swelling properties of oligo(poly(ethylene glycol) fumarate) hydrogels for cartilage tissue engineering. *J. Biomed. Mater. Res.* **2002**, *59* (3), 429–437.
- Temenoff, J. S.; Mikos, A. G. Injectable biodegradable materials for orthopedic tissue engineering. *Biomaterials* **2000**, *21* (23), 2405–2412.
- Martens, P. J.; Metters, A. T.; Anseth, K. S.; Bowman, C. N. A generalized bulk-degradation model for hydrogel networks formed from multivinyl cross-linking molecules. *J. Phys. Chem. B* **2001**, *105*, 5131–5138.
- Metters, A. T.; Anseth, K. S.; Bowman, C. N. A statistical kinetic model for the bulk degradation of PLA-*b*-PEG-*b*-PLA hydrogel networks: Incorporating network nonidealities. *J. Phys. Chem. B* **2001**, *105* (34), 8069–8076.

- (23) Metters, A. T.; Anseth, K. S.; Bowman, C. N. A statistical kinetic model for the bulk degradation of PLA-*b*-PEG-*b*-PLA hydrogel networks. *J. Phys. Chem. B* **2000**, *104* (30), 7043–7049.
- (24) Martens, P. J.; Bryant, S. J.; Anseth, K. S. Tailoring the degradation of hydrogels formed from multivinyl poly(ethylene glycol) and poly(vinyl alcohol) macromers for cartilage tissue engineering. *Biomacromolecules* **2003**, *4* (2), 283–292.
- (25) West, J. L.; Hubbell, J. A. Polymeric biomaterials with degradation sites for proteases involved in cell migration. *Macromolecules* **1999**, *32* (1), 241–244.
- (26) Elbert, D. L.; Pratt, A. B.; Lutolf, M. P.; Halstenberg, S.; Hubbell, J. A. Protein delivery from materials formed by self-selective conjugate addition reactions. *J. Controlled Release* **2001**, *76* (1–2), 11–25.
- (27) Lutolf, M. P.; Lauer-Fields, J. L.; Schmoekel, H. G.; Metters, A. T.; Weber, F. E.; Fields, G. B.; Hubbell, J. A. Synthetic matrix metalloproteinase-sensitive hydrogels for the conduction of tissue regeneration: Engineering cell-invasion characteristics. *Proc. Natl. Acad. Sci. U.S.A.* **2003**, *100* (9), 5413–5418.
- (28) Lutolf, M. P.; Raeber, G. P.; Zisch, A. H.; Tirelli, N.; Hubbell, J. A. Cell-responsive synthetic hydrogels. *Adv. Mater.* **2003**, *15* (11), 888–892.
- (29) Lutolf, M. P.; Weber, F. E.; Schmoekel, H. G.; Schense, J. C.; Kohler, T.; Muller, R.; Hubbell, J. A. Repair of bone defects using synthetic mimetics of collagenous extracellular matrixes. *Nat. Biotechnol.* **2003**, *21* (5), 513–518.
- (30) Rydholm, A. E.; Bowman, C. N.; Anseth, K. S. Degradable thiol-acrylate photopolymers: Polymerization and degradation behavior of an *in situ* forming biomaterial. *Biomaterials* **2004**, *26* (22), 4495–4506.
- (31) Reddy, S. K.; Anseth, K. S.; Bowman, C. N. Modeling of network degradation in mixed step-chain growth polymerization. *Polymer* **2005**, *46* (12), 4212–4222.
- (32) DuBose, J. W.; Cutshall, C.; Metters, A. T. Controlled release of tethered molecules via engineered hydrogel degradation: Model development and validation. *J. Biomed. Mater. Res.* **2005**, *74A*, 104–116.
- (33) Cramer, N. B.; Bowman, C. N. Kinetics of thiol-ene and thiol-acrylate photopolymerizations with real-time Fourier transform infrared. *J. Polym. Sci., Part A: Polym. Chem.* **2001**, *39* (19), 3311–3319.
- (34) Sawhney, A. S.; Pathak, C. P.; Hubbell, J. A. Bioerodible hydrogels based on photopolymerized poly(ethylene glycol)-*co*-poly( $\alpha$ -hydroxy acid) diacrylate macromers. *Macromolecules* **1993**, *26* (4), 581–587.
- (35) Berchtold, K. A.; Nie, J.; Stansbury, J. W.; Hacıoglu, B.; Beckel, E. R.; Bowman, C. N. Novel monovinyl methacrylic monomers containing secondary functionality for ultrarapid polymerization: Steady-state evaluation. *Macromolecules* **2004**, *37* (9), 3165–3179.
- (36) Berchtold, K. A.; Bowman, C. N. In *RadTech Europe 99 Conference Proceedings*, Berlin, Germany, 1999; p 767.
- (37) Metters, A. T.; Anseth, K. S.; Bowman, C. N. Fundamental studies of a novel, biodegradable PEG-*b*-PLA hydrogel. *Polymer* **2000**, *41* (11), 3993–4004.
- (38) Flory, P. J. *Principles of Polymer Chemistry*; Cornell University Press: Ithaca, NY, 1953.
- (39) Lecamp, L.; Houllier, B.; Youssef, B.; Bunel, C. Photoinitiated crosslinking of a thiol-methacrylate system. *Polymer* **2001**, *42*, 2727–2736.
- (40) Elliott, J. E.; Anseth, K. S.; Bowman, C. N. Kinetic modeling of the effect of solvent concentration on primary cyclization during polymerization of multifunctional monomers. *Chem. Eng. Sci.* **2001**, *56* (10), 3173–3184.

BM0603793